Entanglement topology of two qubits

Dong Zhou, Gia-Wei Chern, Jianjia Fei, and Robert Joynt Physics Department, University of Wisconsin-Madison, Madison, Wisconsin 53706, USA (Dated: June 7, 2019)

We introduce the notion of entanglement topology, which is related to whether both the entangled and separable states have finite volumes in the relevent physical space of the dynamics. Quantitative geometric picture for the two-qubit state space are constructed using coherence vector representation and thus system dynamics can be visualized. In spite of the high dimensionality and geometric complexity of the full state space, decoherence process might only probe a lower dimensional subspace with relatively simple structure, which we call dynamical subspaces. Entanglement evolution is determined by the entanglement topology of the corresponding dynamical subspaces, and the entanglement property of the limiting state. Various physically relevant examples are demonstrated.

PACS numbers: 02.40.Pc, 03.65.Ud, 03.65.Yz, 03.67.Mn

I. INTRODUCTION

Entanglement is one of the most intriguing aspect of quantum physics. Being a useful resource for quantum computation and communication [1, 2], its structure and behavior are not fully understood even for simple systems such as two qubits where computable entanglement measure such as Wootter's concurrence is available [3]. The difficulty resides in the high dimensionality of state spaces (fifteen for two qubits) and non-analyticity of the definition of the entanglement measure.

In the presence of unwanted but inevitable interactions between the quantum system and environment, commonly known as decoherence, quantum coherence as well as entanglement degrade. Apart from the expected half-life (HL) decaying behavior, sudden disappearance of entanglement has been theoretically predicted and experimentally observed [4, 5]. Widely known as entanglement sudden death (ESD), it is shown to be a generic behavior of multipartite quantum systems regardless of whether the environment is modeled as quantum or classical, Markovian or non-Markovian [6–19]. Entanglement sudden birth (ESB) is also reported and is believed to be related to the memory effect of the (non-Markovian) environment [6, 18–21]. Although most investigations have been focused on two-qubit systems, ESD and ESB have been shown to exist in multi-qubit systems, and even quantum systems with infinite dimensional Hilbert spaces, such as hamonic oscillators [22–28].

The universality of the various entanglement behaviors indicates that they are derived from some structual property of the state space with respect to entanglement and the system dynamics can be viewed as a probe to that property. We will refer to it as entanglement topology. A state space M is said to possess non-trivial entanglement topology if both the set S formed by separable states and the set $M\backslash S$ formed by entangled states occupy finite volume. In other words, both the entangled and separable states form dense sets in M. Using a phase-space-like argument, where any physical state, entangled or separable, is represented by a point and any (decoherence) dynamics is visualized as a path in the state

space, the existence of ESD/ESB can be explained by the fact that the state space of the quantum system has non-trivial entanglement topology [29–32]. ESD happens when the state trajectory passes the boundary of entangled and separable regions from the entangled side. Likewise, ESB can be explained by the state trajectory crossing the separable-entangled boundary from the separable side. Using a natural measure in the space of two-qubit density matrices, Zyczkowski et.al. showed that the separable states occupy more than half the volume of the full state space [32]. Thus the two-qubit state space Mhas non-trivial entanglement topology and ESD/ESB is a generic behavior for two-qubit systems. A more intuitive parametrization of the multi-qubit state space is the coherence (generalized Bloch) vector representation, where a one-to-one correspondence is constructed for any density matrix ρ and a point \vec{n} in a convex set inside a high dimensional ball [33–35]. We recently pointed out that two characters of any model determines the entanglement behaviors: the dynamical subspace D and the limiting state \vec{n}_{∞} [31]. $D \subseteq M$ is where the evolutions $\vec{n}(t)$ take place and is determined by both the initial state and the decoherence process. $\vec{n}_{\infty} = \lim_{t \to \infty} \vec{n}(t)$ and we limit ourselves to the cases where $\vec{n}_{\infty} \in S$ exists. Multiple limiting states and entangled \vec{n}_{∞} has been considered in Ref. [30, 36].

As a result of the entanglement topology of D and the entanglement property of \vec{n}_{∞} , only four types of entanglement evolutuion are possible, as seen in Fig.1 [31]. Entanglement evolutions in category A approach the boundary of separable and entangled regions asymptotically from the entangled side. The state trajectories never hit the separable region while the decreasement in entanglement may or may not be monotonic, as seen in Ref. [37]. Entanglement evolutions in category \mathcal{B} bounce off the bouldary of separable and entangled regions at finite times but never enter the separable region S. Overall, entanglement deminishes nonmonotonically. Entanglement evolutions in category \mathcal{E} enter S at finite time and entanglement stays zero afterwards. This is the typical ESD behavior. Entanglement evolutions in category \mathcal{O} enbrace ESB. After ESD, entanglement suddenly

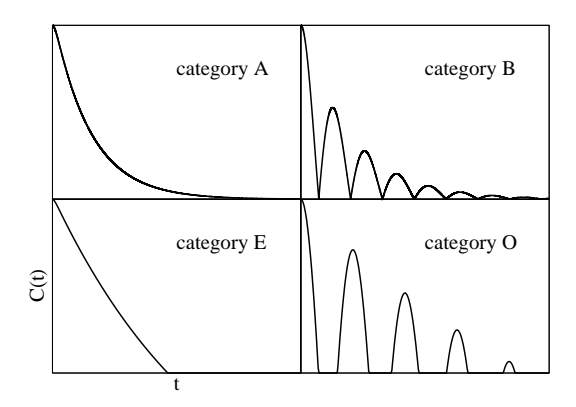


FIG. 1. Four categories of entanglement evolution. A: approaching. B: bouncing. \mathcal{E} : entering. \mathcal{O} : oscillating.

appears after some dark period. Note if D has trivial entanglement topology, i.e. $D \cap S$ is of zero volume in D, only entanglement evolutions in categories \mathcal{A} and \mathcal{B} can happen. On the other hand, if D has non-trivial entanglement topology, i.e. $D \cap S \subset D$ is of finite volume, all four categories are possible and \vec{n}_{∞} is decisive in determining the category.

In this paper, we further develop these ideas in Ref. [31] to provide quantitative geometric picture for the twoqubit state space and dynamics using coherence vector representation. The paper is organized as follows: In Sec. II, we introduce the coherence vector representation for the two qubit case and show how to describe decoherence dynamics in terms of a transfer matrix acting on the state (coherence) vector. In Sec. III, we characterize the entanglement structure of the full fifteen dimensional two-qubit state space M. Monte Carlo studies show that M has non-trivial entanglement topology, just as in Ref. [32]. Thus ESD and ESB are generic behavior for two-qubit disentanglement dynamics. In Sec. IV and V, we construct three dimensional and eight dimensional dynamical subspaces D that have trivial entanglement topology. In Sec. VI and VII, we show physical deocherence processes could induce dynamical subspaces D that are on the one hand of lower dimension than M, on the other hand have non-trivial entanglement topology. We finally conclude our results in Sec. VIII.

II. COHERENCE VECTOR AND DECOHERENCE DYNAMICS

It is well-known that any (mixed) state of a two-level system can be visualized as a real three dimensional vector in a ball - the Bloch vector representation. Pure states live on the the unit sphere while mixed states are inside the sphere. Apart from an overal phase, there is a one-to-one correspondence between the quantum states and points in this ball. The same idea applies to any N-level quantum systems and one can define the coherence vector, or generalized Bloch vector via the density matrix

decomposition [33–35]

$$\rho = \frac{1}{N} I_N + \frac{1}{N} \sum_{i=1}^{N^2 - 1} n_i \mu_i, \tag{1}$$

where I_N is the N dimensional identity matrix and $n_i = \operatorname{Tr} \rho \mu_i$ are the components of the coherence vector. μ_i are elements of su(N) algebra satisfying $\mu_i = \mu_i^{\dagger}$, $\operatorname{Tr} \mu_i = 0$, $\operatorname{Tr} \mu_i \mu_j = N \delta_{ij}$. Note n_i are real and $\operatorname{Tr} \rho^2 \leq 1$. The state space is a subset of a ball in \mathbb{R}^{N^2-1} . For the su(2) case, this is the famous Bloch ball.

For $N \geq 3$, it turns out that not all points inside the ball are permissible quantum states. This is because Tr $\rho^2 \leq 1$ is only a neccesary condition for the density matrix to be positive when $N \geq 3$. Complete positivity, that is all the eigenvalues of the density matrix being non-negative, requires all coefficients a_i of the characteristic polynomial $\det(xI_N-\rho)$ to be non-negative [33]. For two-qubit systems there are four of them, which are

$$1!a_1 = \text{Tr } \rho = 1,$$

$$2!a_2 = 1 - \text{Tr } \rho^2,$$

$$3!a_3 = 1 - 3\text{Tr } \rho^2 + 2\text{Tr } \rho^3,$$

$$4!a_4 = 1 - 6\text{Tr } \rho^2 + 8\text{Tr } \rho^3 + 3\left(\text{Tr } \rho^2\right)^2 - 6\text{Tr } \rho^4.$$

When translated to the coherence vector representation, those constraints give rise to complicated geometric shape for the physical space M in \mathbb{R}^{15} . Note $a_2 \geq 0$ is equivalent to Tr $\rho^2 \leq 1$ and is only a necessary condition for positivity except for N=2 (single qubit) case. For two qubits, Tr $\rho^2 \leq 1$ is translated into $n^2 \leq 3$, i.e. the state space M is a subset of a ball in \mathbb{R}^{15} where pure states live on the sphere.

For two qubits, the density matrix can be decomposed into linear combinations of the elements of the Lie algebra $\mathfrak{su}(4)$

$$\rho = \frac{1}{4}I_4 + \frac{1}{4}\sum_{i=1}^{15} n_i \mu_i, \tag{2}$$

The su(4) elements can be considered as bases vectors and the expansion coefficients n_i form a fifteen dimensional vector, providing full description of the (mixed) quantum state. Note the fully mixed state $\rho = I_4/4$ is given by $\vec{n} = \mathbf{0}$, i.e. the origin of \mathbb{R}^{15} .

We choose the bases to be $\sigma_{\mu} \otimes \sigma_{\nu}$ with $\mu, \nu = 0, 1, 2, 3$ where σ are Pauli matrices. We exclude $I_4 = \sigma_0 \otimes \sigma_0$. This particular choice has the properties

$$\mu_i = \mu_i^{\dagger}, \text{Tr } \mu_i = 0, \text{Tr } \mu_i \mu_j = 4\delta_{ij}. \tag{3}$$

We note different normalizations are used in the literature [33–35].

The fifteen coherence vector components can be considered as two ploar vectors and a 3×3 correlation matrix

[38, 39],

$$\vec{P}_A = \begin{bmatrix} n_4 \\ n_8 \\ n_{12} \end{bmatrix} = \begin{bmatrix} n_{XI} \\ n_{YI} \\ n_{ZI} \end{bmatrix} = \begin{bmatrix} \langle XI_2 \rangle \\ \langle YI_2 \rangle \\ \langle ZI_2 \rangle \end{bmatrix}, \tag{4}$$

$$\vec{P}_B = \begin{bmatrix} n_1 \\ n_2 \\ n_3 \end{bmatrix} = \begin{bmatrix} n_{IX} \\ n_{IY} \\ n_{IZ} \end{bmatrix} = \begin{bmatrix} \langle I_2 X \rangle \\ \langle I_2 Y \rangle \\ \langle I_2 Z \rangle \end{bmatrix}, \tag{5}$$

$$Q = \begin{bmatrix} n_5 & n_6 & n_7 \\ n_9 & n_{10} & n_{11} \\ n_{13} & n_{14} & n_{15} \end{bmatrix} = \begin{bmatrix} \langle XX \rangle & \langle XY \rangle & \langle XZ \rangle \\ \langle YX \rangle & \langle YY \rangle & \langle YZ \rangle \\ \langle ZX \rangle & \langle ZY \rangle & \langle ZZ \rangle \end{bmatrix}. \quad (6)$$

Here X, Y, Z are Pauli matrices and we explicitly write the coherence vector components as the expectation values of the observables.

Dynamics are described by transfer matrices T(t) acting on the initial coherence vector $\vec{n}(0)$, i.e.

$$\vec{n}(t) = T(t) \ \vec{n}(0). \tag{7}$$

Coherent dynamics are described by unitary transformations on the density matrix thus orthogonal matrix acting on the coherence vector, while decoherence dynamics are characterized by the nonorthogonality of the transfer matrix. The length of \vec{n} decreases to zero unless symmetries introduce conservation laws for its components. $n = |\vec{n}|$ denotes purity of the state.

In the case of non-interacting qubits, the two-qubit dynamics can be decomposed into single-qubit dynamics [19]. The extended two-qubit transfer matrix is $\underline{T}(t) = \underline{R}^A \otimes \underline{R}^B$ where

$$\underline{R}(t) = \begin{bmatrix} 1 & 0 & 0 & 0 \\ 0 & \zeta(t)\cos B_0 t & \zeta(t)\sin B_0 t & 0 \\ 0 & -\zeta(t)\sin B_0 t & \zeta(t)\cos B_0 t & 0 \\ 0 & 0 & 0 & e^{-\Gamma_1 t} \end{bmatrix}$$
(8)

is the extended transfer matrix of individual qubits. The top left 1 describes the dynamics of σ_0 and is there only to match dimension. Here $\zeta(t)$ describes dephasing process, Γ_1 is the longitudinal relaxation rate and B_0 is static field in the z direction that causes Larmor precession. $\zeta(0)=1$ and $\zeta(\infty)=0$ if dephasing occurs. Note this dynamical description of decoherence is completely general as long as one can separate dephasing and relaxation channels.

To quantify the two-qubit entanglement, we use Wootter's concurrence for its ease of calculation [3]. The concurrence varies from 0 for separable states to 1 for the maximally entangled state, i.e. Bell-like states. It is defined as $C^{AB} = \max\{0, q\}$, and

$$q = \lambda_1 - \lambda_2 - \lambda_3 - \lambda_4 , \qquad (9)$$

where λ_i are the square roots of the eigenvalues of the matrix $\rho_{AB}\tilde{\rho}_{AB}$ arranged in decreasing order and

$$\tilde{\rho}_{AB} = (\sigma_y^A \otimes \sigma_y^B) \rho_{AB}^* (\sigma_y^A \otimes \sigma_y^B), \tag{10}$$

is the spin-flip operation on the density matrix. ρ_{AB}^* is the complex conjugate of the density matrix ρ_{AB} .

	1	2	3	4	5	6	7	8	9	10	11	12	13	14
ZZ 15	В	В	Α	В	Α	Α	В	В	Α	Α	Α	Α	В	В
ZY 14	В	Α	В	В	Α	В	Α	В	A	В	Α	Α	В	
ZX 13	Α	В	В	В	В	Α	Α	В	В	Α	Α	Α		
ZI 12	Α	Α	Α	В	В	В	В	В	В	В	В			
YZ 11	В	В	Α	В	Α	Α	В	Α	В	В				
YY 10	В	Α	В	В	Α	В	Α	Α	В					
YX 9	Α	В	В	В	В	A	Α	Α						
YI 8	Α	Α	A	В	В	В	В							
XZ 7	В	В	A	Α	В	В								
XY 6	В	Α	В	Α	В									
XX = 5	Α	В	В	Α										
XI 4	Α	Α	A											
IZ = 3	В	В												
IY 2	В													

TABLE I. Two dimensional sections Σ_2 of the full two-qubit state space M, keeping only two components of the coherence vector non-zero. Type A is the square section, while type B is the disc section.

III. FULL STATE SPACE M

In the simplest and most general senario, the decoherence dynamics possesses no symmetry at all and the quantum system is eventually driven to the fully mixed state $\vec{n}_{\infty} = \mathbf{0}$. The dynamical subspace D is equal to the full state space M. We thus need to address the entanglement topology of M in order to understand the most general disentanglement processes.

A general quantum state is separable if its density matrix can be decomposed into convex combination of product states, i.e.

$$\rho = \sum_{k} p_k \rho_k^A \otimes \rho_k^B, \tag{11}$$

where $p_k \geq 0$ and $\sum_k p_k = 1$ [40]. Thus the set S of separable states is a convex since any convex combination of separable state is also separable. Similarly, the state space M is convex as well.

Concurrence is zero along any of the fifteen bases directions. Along directions $n_{IX,IY,IZ,XI,YI,ZI}$, i.e. those that correspond to the components of the polar vectors, the coherence vector components have range $[-\sqrt{3},\sqrt{3}]$. In the other coherence vector directions, i.e. those that correspond to the correlation matrix Q, the range is only [-1,1].

We make two-dimensional sections Σ_2 of M with two and only two components of \vec{n} non-zero. In contrast to Ref. [41] where generalized Gell-Mann matrices are used for the elements of su(4) algebra, we find only two types of sections, as seen in Fig. 2. Σ_2 is either a square or a disc. All states in those sections are separable since they can be expressed by linear combinations of the bases vector. All possible combinations of sections Σ_2 are listed in Tab. I.

The analytical approach presented above only gives a glimpse into the structure of the full state space M. In

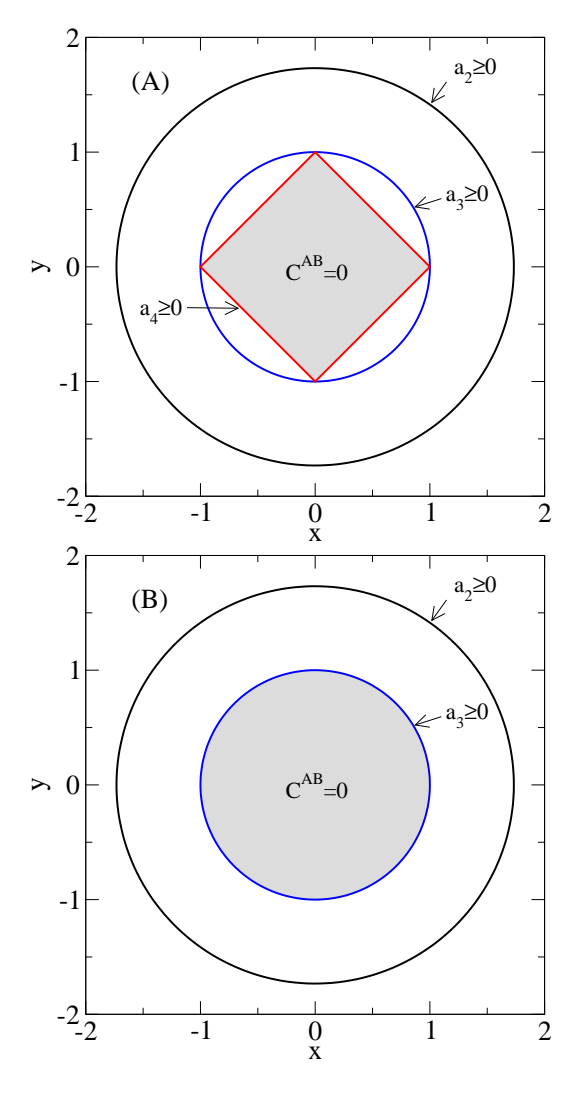


FIG. 2. (Color online) Two dimensional section Σ_2 of the full two-qubit state space M. Only two inequivalent sections are possible and in both cases, the full section is filled with separable states.

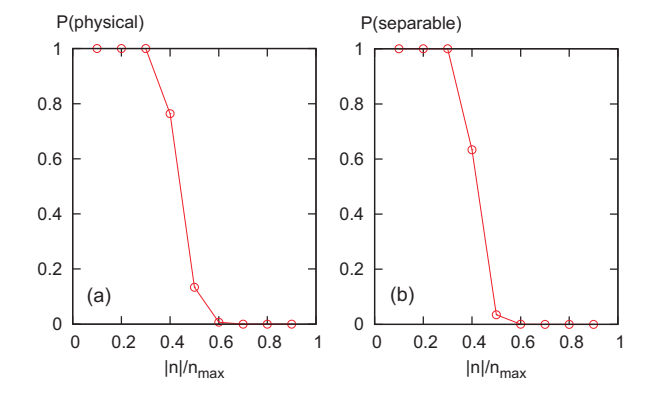


FIG. 3. Radial distribution of (a) physical states in the ball of radius $\sqrt{3}$ in \mathbb{R}^{15} and (b) separable states in the two-qubit state space M.

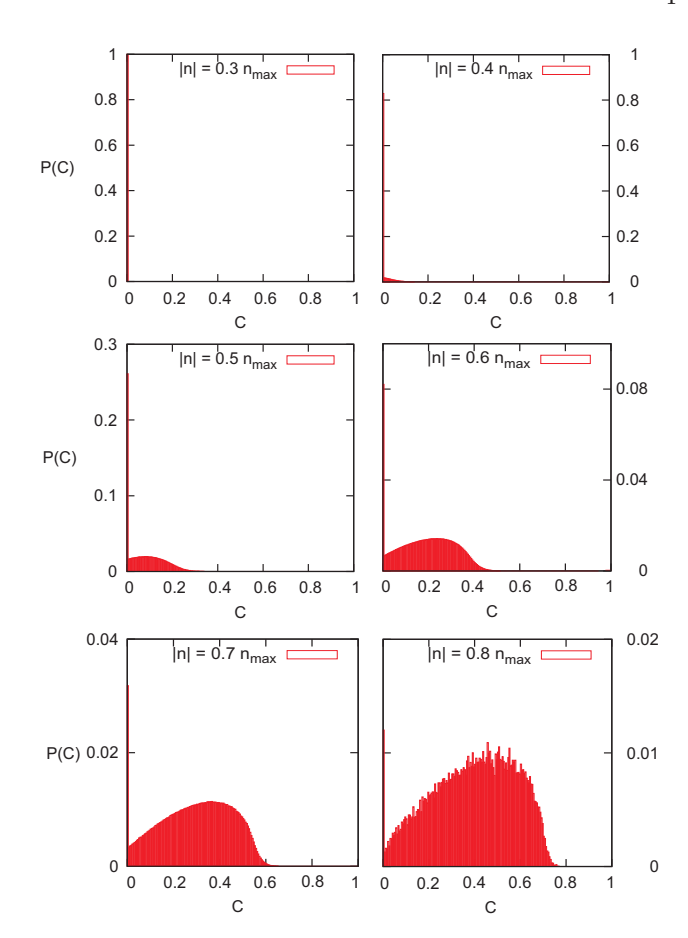


FIG. 4. Concurrence distribution of the physical states at different radius $|\vec{n}|$.

order to gain a better understanding of the geometrical structure of M and the set S of separable states in the coherence vector representation, we performed Monte Carlo simulations on the \mathbb{R}^{15} ball. The two-qubit state space M is inscribed to the sphere of radius $\sqrt{3}$ in \mathbb{R}^{15} . Thus a 15-component vector \vec{n} is randomly generated with length $|\vec{n}| \leq n_{\text{max}} = \sqrt{3}$. Since not all points inside the sphere represent valid physical states, we first check whether the density matrix constructed using the chosen \vec{n} satisfies the positivity condition. Fig. 3(a) shows the radial distribution of the probability of finding a valid physical state at a given length $|\vec{n}|$. For a permissible vector \vec{n} , we then proceed to compute the concurrence of the corresponding quantum state. The probability of finding a separable state (with C=0) as a function of length $|\vec{n}|$ is shown in Fig. 3(b). Both distributions drops quickly as $|\vec{n}|$ increases.

We also numerically compute the probability P(C) of finding a physical state with concurrence C for various fixed lengths $|\vec{n}|$ of the Bloch vector. As the radius increase, the percentage of entangled states increases, as seen in Fig. 4. At radius $n = n_{\text{max}}/2$, about a quarter of the physical states are separable while at $n = \frac{4}{5}n_{\text{max}}$, separable states only accounts for one percent of the physical states. In addition, all states are separable near the

origin **0**. It is known that S contains a ball of separable states with radius $1/\sqrt{3}$ centered around the origin **0** and our numerical study gives an upper bound 0.6222 on the radius r_S of maximum inscribed ball of M formed by separable states.

Thus we see the full two-qubit state space M has non-trivial entanglement topology and the structures of both M and S are complicated. Fortunately physical dynamics may happen in dynamical subspaces with lower dimension and simpler geometric structure. This simplicity in the dynamical subspaces D is the focus of the following four sections.

IV. D_3 WITH TRIVIAL ENTANGLEMENT TOPOLOGY

Here we introduced a dynamical subspace D_3 that is three dimensional and can be induced from a physical model where the two qubits are interacting with each other with Heisenberg interactions. Decoherence is caused by one qubit being subjected to random telegraph noise (RTN). D_3 is a ball with trivial entanglement topology and thus can only support entanglement evolutions in categories \mathcal{A} and \mathcal{B} , as seen in Fig. 6.

If the two-qubit Hamiltonian does not connect the $\{|00\rangle, |11\rangle\}$ states with the $\{|01\rangle, |10\rangle\}$ states and the initial density matrix has the same structure, the four-level problem decouples into two-level problems and we can use the Bloch ball representation to visualize the state space and entanglement evolution.

We consider states whose density matrices have only 2×2 non-zero blocks on either $\{|00\rangle, |11\rangle\}$ or $\{|01\rangle, |10\rangle\}$. Thus only one Bloch ball is needed to represent the dynamical subspace D.

The square roots of the non-zero eigenvalues of $\rho\tilde{\rho}$ are $\lambda_{1,2} = (\sqrt{1-r^2\cos^2\theta} \pm r\sin\theta)/2$, where r and θ are the spherical coordinates of the Bloch ball, and $\tilde{\rho}$ is the spin-flip operation, as in Eq. 10. The concurrence is given by

$$C^{AB} = r\sin\theta. \tag{12}$$

The maximally entangled states are on the equator and the separable states are on the z-axis, as seen in Fig. 5. The concurrence has azimuthal symmetry and is linear in the radial distance.

Note the separable states form a lower dimensional manifold thus D_3 has trivial entanglement topology. The trajectories of the quantum state either hit $D_3 \cap S$ at discrete time instants which puts them in category \mathcal{B} , or approaches it asymptotically which puts them in category \mathcal{A} . We now construct a concrete model to demonstrate how those two qualitatively different behaviors are related to the memory effect of the noise, i.e. Markovian noise gives rise to the approaching behavior while Non-Markovian noise causes the bouncing behavior.

Suppose the two qubits are interacting with each other with Heisenberg interaction J. Qubit A sees a static field

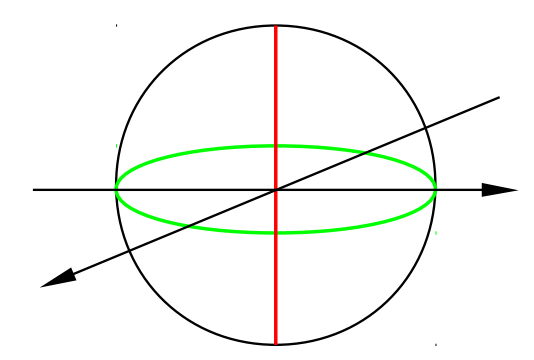


FIG. 5. (Color online) Effective Bloch sphere representation for the dynmaical subspace D_3 . The north and south pole are either $\{|10\rangle, |01\rangle\}$ or $\{|00\rangle, |11\rangle\}$. States resting on the red line connecting north and south pole have zero concurrence. States on the green equator are equivalent to Bell states thus maximally entangled.

 B_0 while qubit B sees a fluctuating field s(t)g, both in the z direction. s(t) assumes value ± 1 and switches between these two values with rate γ . It is known as RTN and is widely observed in solid state systems [42–45]. The Hamiltonian is time-dependent and can be written as

$$H(t) = -\frac{1}{2} \left[\frac{J}{2} \vec{\sigma}^A \cdot \vec{\sigma}^B + s(t) g \sigma_z^B + B_0 \sigma_z^A \right], \qquad (13)$$

where σ 's are Pauli matrices.

For this dephasing noise model, the fore-mentioned decoupling into two two dimensional subspaces occurs. In the 2×2 block labelled by $\{|00\rangle, |11\rangle\}$,

$$H(t) = -\frac{\sigma_z}{2} [s(t)g + B_0].$$
 (14)

This Hamiltonian can be solved exactly using a quasi-Hamiltonian method [35]. The time-dependent decoherence problem can be mapped exactly to a timeindependent problem where the two-value fluctuating field is described by a spin half particle. The quasi-Hamiltonian is given by

$$H_q = -i\gamma + i\gamma\tau_1 + L_z(B_0 + \tau_3 g), \tag{15}$$

where τ_i are the Pauli matrices of the noise 'particle'. L_z is the SO(3) generator in z direction.

The transfer matrix is given by

$$T(t) = \begin{bmatrix} \zeta_T(t)\cos B_0 t & \zeta_T(t)\sin B_0 t & 0\\ -\zeta_T(t)\sin B_0 t & \zeta_T(t)\cos B_0 t & 0\\ 0 & 0 & 1 \end{bmatrix}$$
(16)

where

$$\zeta_T(t) = e^{-\gamma t} \left[\cos(\Omega t) + \frac{\gamma}{\Omega} \sin(\Omega t) \right]$$
 (17)

$$\Omega = \sqrt{g^2 - \gamma^2} \tag{18}$$

is the dephasing function due to RTN and it describes the phase coherence in the x-y plane [19]. Note $\zeta_T(t)$ has

qualitatively different behaviors in the non-Markovian $(g > \gamma)$ and Markovian $(g > \gamma)$ regions, as the trigonometric functions become hyperbolic functions [35].

Taking $|\Phi+\rangle=(|00\rangle+|11\rangle)/\sqrt{2}$ as initial state, the effective Bloch vector is

$$\vec{n}(t) = \begin{bmatrix} \zeta_T(t)\cos B_0 t \\ -\zeta_T(t)\sin B_0 t \\ 0 \end{bmatrix}. \tag{19}$$

The state trajectory is fully in the equatorial plane, as seen in Fig. 6. The dephasing function $\zeta_T(t)$ modulates the radial variation and the static field B_0 provides precession. In the Markovian case, the monotonicity of ζ_T gives rise to spiral while in the non-Markovian case the state trajectory periodically spirals outwards with frequency Ω . In both cases, the limiting state $\vec{n}_{\infty} = \mathbf{0}$.

The concurrence evolution is given by

$$C^{AB}(t) = |\zeta_T(t)|. \tag{20}$$

Thus Markovian noise gives rise to entanglement evolutions in category \mathcal{A} while non-Markovian noise gives rise to that in category \mathcal{B} . Entanglement evolutions in the

other two categories can not occur due to the triviality of the entanglement topology of D_3 .

V. D_8 WITH TRIVIAL ENTANGLEMENT TOPOLOGY

In the previous section we see that dynamical subspaces spanned by two computational bases states does not possess non-trivial entanglement topology. A natual question is whether increasing the number of bases helps. Here we choose the Hamiltonian to connect only the states spanned by $\{|00\rangle, |01\rangle, |10\rangle\}$. All other possible combinations are equivalent to this choice by renaming the 0 and 1 states.

Using Gell-Mann matrices as the elements of su(3) algebra, the state space is a subset of a ball in \mathbb{R}^8 [33].

$$\rho = \frac{1}{2}I + \frac{1}{2}\sum_{i=1}^{8} n_i \mu_i \tag{21}$$

and μ_i satisfies

$$\mu_i = \mu_i^{\dagger}, \quad \text{Tr } \mu_i = 0, \quad \text{Tr } \mu_i \mu_j = 2\delta_{ij}.$$
 (22)

The square roots of the eivenvalues of $\rho \tilde{\rho}$ are

$$\lambda_{1,2} = \left| \frac{1}{2} \sqrt{n_6^2 + n_7^2} \pm \frac{\sqrt{2}}{6} \sqrt{2 - \sqrt{3} \left(\sqrt{3} n_3 + n_8 \right) + 3n_8 \left(\sqrt{3} n_3 - n_8 \right)} \right|, \quad \lambda_{3,4} = 0 \tag{23}$$

Thus the set $D_8 \cap S$ of separable states is composed of two geometric objects: $n_6 = n_7 = 0$ which is in \mathbb{R}^6 and

$$2 - \sqrt{3} \left(\sqrt{3}n_3 + n_8 \right) + 3n_8 \left(\sqrt{3}n_3 - n_8 \right) = 0$$

which is in \mathbb{R}^7 . In addition to a concurrence-zero hyperline we have a concurrence-zero hyperplane in D_8 . D_8 remains to have trivial entanglement topology and only supports entanglement evolutions in categories \mathcal{A} and \mathcal{B} .

Introducing extra dimension thus helps to form non-trivial entanglement topology but a Hilbert space spanned by three of the four computational bases is still not enough. The reason both D_3 and D_8 fail to possess non-trivial entanglement topology is because they avoid the region near the fully mixed state $\mathbf{0}$, where most separable states reside in [46]. This region can be included with the dynamical subspaces in the next two sections.

VI. ZJ_5 WITH NON-TRIVIAL ENTANGLEMENT TOPOLOGY

Here we present a physically motivated dynamical subspace where the decoherence process satisfies the following conditions: 1) the two qubits are not interacting; 2) the noises on the qubits are not correlated; 3) the effect of dephasing and relaxation are separable; 4) the initial state is in this space.

The first two conditions simplifies the two-qubit dynamics to single-qubit dynamics. The third condition means one can use Eq. 8 to describe single qubit dynamics where $\zeta(t)$ and Γ_1 characterize dephasing and relaxation respectively.

It is a specially parametrized five dimensional section of the full two-qubit state space M. Only the components n_{XX} , n_{XY} , n_{YX} , n_{YY} and n_{ZZ} are non-zero and we further have constraints $n_{XX} = n_{YY}$ and $n_{XY} = -n_{YX}$. We thus use $n_{XX,XY,ZZ}$ as independent parameters and the state space can be visualized in three dimensions. This dynamical subspace has been previously considered in Ref. [31] and we will call it ZJ_5 for simplicity.

Note $n_{XX}^2 + n_{XY}^2 = R^2$ is conserved in ZJ_5 . The

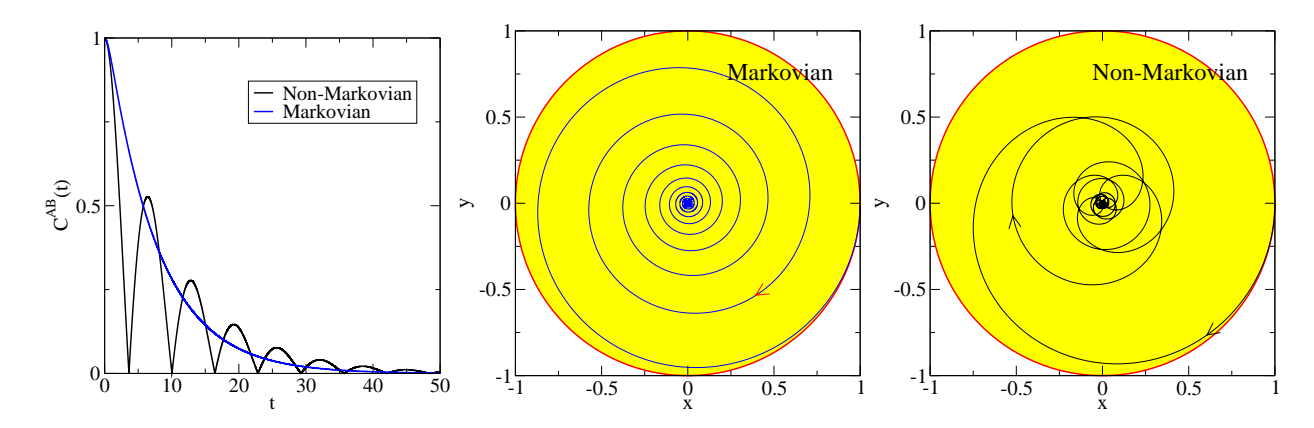


FIG. 6. Entanglement evolution and state trajectories in the dynamical subspace D_3 with RTN in the Markovian and Non-Markovian regions. Concurrence is equal to the absolute value of $\zeta_T(t)$. State trajectory in the equatorial plane of the effective Bloch representation where the only separable state is the origin **0**. The initial state is the Bell state $|\Phi+\rangle$. The concurrence is given by the radial distance. In both cases, g=0.5, $B_0=1$. $\gamma=1$ for the Markovian case and $\gamma=0.1$ for the Non-Markovian case.

positivity of the density matrix requires

$$a_2 \ge 0 \implies 2R^2 + n_{ZZ}^2 \le 3$$
 (24)

$$a_3 \ge 0 \implies n_{ZZ} \le 1 - 2R^2$$
, and $n_{ZZ} \ge -1$ (25)

$$a_4 > 0 \implies 2R + n_{ZZ} < 1$$
 (26)

The concurrence is given by

$$C^{AB} = \max\left\{0, R - \frac{1 + n_{ZZ}}{2}\right\}. \tag{27}$$

Separable states form a spindle shape on top and entangled states form a torus-like shape on bottom with triangular cross sections. A section along $n_{XY}=0$ is shown in Fig. 7.

We have thus fully described the entanglement topology of ZJ_5 and now we construct entanglement evolutions that induce ZJ_5 . As we said, ZJ_5 can be induced by very general type of disentanglement processes. To be more specific, we use similar model as Eq. 13

$$H(t) = -\frac{1}{2} \left[s(t) \vec{g} \cdot \vec{\sigma}^B + B_0 \sigma_z^A \right],$$
 (28)

Note the RTN has both dephasing and relaxation effect in this case. Situations with $n_{XY} = 0$ at intermediate qubit working point (with the presence of both dephasing and relaxation noise) has been considered in Ref. [31]. Here we choose the initial state to be the generalized Werner state [40]

$$w_r^{\Phi} = r |\Phi\rangle \langle \Phi| + \frac{1-r}{4} I_4, \qquad (29)$$

where

$$|\Phi\rangle = \frac{1}{2} \left(|00\rangle + e^{i\phi} |11\rangle \right)$$
 (30)

is a Bell state.

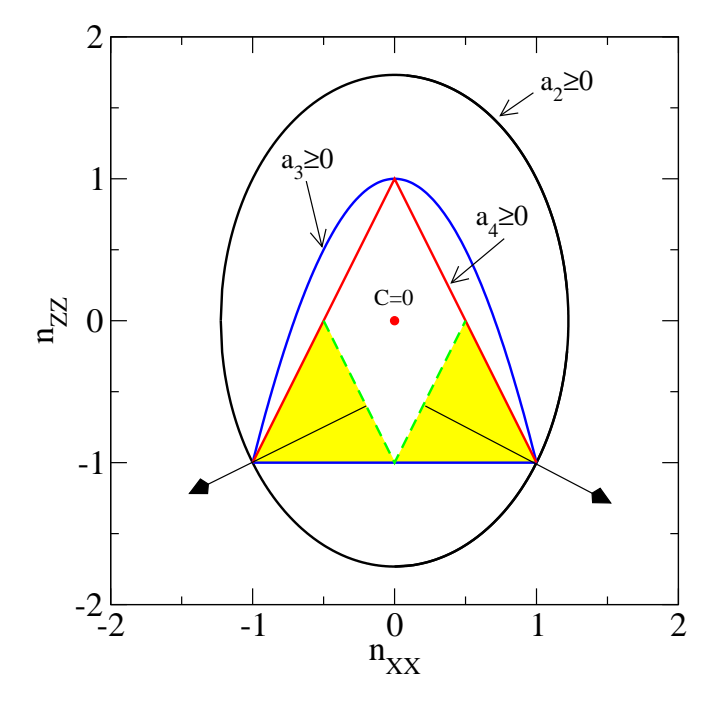


FIG. 7. (Color online) Cross section of the dynamical subspace ZJ_5 with $n_{XY}=0.$ $a_2\geq 0$ is the eclipse. $a_3\geq 0$ gives the parabola and the bottom of the isoceles triangle. $a_4\geq 0$ sets the two sides of the triangle. The entangled region is shaded where the filled arrows denote increasing direction of the concurrence. The green dashed line is the boundary of entangled and unentangled states. The fully mixed state is denoted by a red dot.

The state trajectory is then given by

$$n_{XX}(t) = r\cos(2B_0 t)\zeta_T(t),\tag{31}$$

$$n_{XY}(t) = -r\sin(2B_0t)\zeta_T(t), \qquad (32)$$

$$n_{ZZ}(t) = re^{-\Gamma_1 t}. (33)$$

Similarly, if the Werner state derived from the Bell

state

$$|\Psi\rangle = \frac{1}{2} \left(|01\rangle + e^{i\phi} |10\rangle \right) \tag{34}$$

is used as initial state, the state trajectory is

$$n_{XX}(t) = r\zeta_T(t), \tag{35}$$

$$n_{ZZ}(t) = -re^{-\Gamma_1 t}. (36)$$

In both cases, the evolution of the concurrence is

$$C^{AB}(t) = \max\{0, r[|\zeta_T(t)| - \xi(t)]\}$$
 (37)

where $\xi(t) = (1 - re^{-\Gamma_1 t})/2$. Thus dephasing (relaxation) drives the state horizontally (vertically) towards the origin. Note ESD occurs whenever $\xi(t \to \infty) \neq 0$ and the corresponding limiting state is $\vec{n}_{\infty} = \mathbf{0}$ [19]. In the case of pure dephasing, $\Gamma_1 = 0$ and the trajectory moves in the horizontal plane $n_{ZZ} = -r$. The limiting state is $\vec{n}_{\infty} = (0, 0, -r)$. The only case where ESD does not happen is the pure dephasing processes on the $n_{ZZ} = -1$ plane since the separable state is of lower dimension there. This amounts to $\xi(t) = 0$ and there is no abrupt cut-off.

At the pure dephasing point, the exact form of the dephasing function $\zeta_T(t)$ is given by Eq. 17. Entanglement evolutions in categories \mathcal{E} and \mathcal{O} are possible, depending on whether the RTN is Markovian or non-Markovian, as seen in Fig. 8.

If the initial state is on the $n_{ZZ}=-1$ plane, by tuning the relative weight of dephasing and relaxation noise, the entanglement evolution can transit from category \mathcal{A} to category \mathcal{E} if the noise is Markovian, or from category \mathcal{B} to category \mathcal{O} if the noise is non-Markovian [31]. These transitions can be interpreted as a transion of entanglement topology of the dynamical subspace as the physical parameter varies. At the pure dephasing point, ZJ_5 shrinks to the $n_{ZZ}=-1$ disc and becomes a dynamical subspace with trivial entanglement topology.

VII. YE_5 WITH NON-TRIVIAL ENTANGLEMENT TOPOLOGY

Yu and Eberly considered disentanglement process due to spontaneous emission for two two-level atoms in two cavities and found that for specific choices of initial states and decoherence dynamics, ESD occurs [7]. In the coherence vector representation, the dynamical subspace is a five dimensional section of M where the non-zero components are $n_{IZ,XX,YY,ZI,ZZ}$. We call it YE_5 for simplicity. YE_5 has further symmetries $n_{IZ} = n_{ZI}$ and $n_{XX} = n_{YY}$ such that it can also be visualized in three dimentions. Interestingly, the limiting state \vec{n}_{∞} due to spontaneous emission is on the boundary of set S of separable states, in contrast to that of the ZJ_5 case, where \vec{n}_{∞} is typically deep inside S.

The decoherence process is formulated using the Kraus representation

$$\rho(t) = \sum_{\mu=1}^{4} K_{\mu}(t)\rho(0)K_{\mu}^{\dagger}(t), \tag{38}$$

where the Kraus operators $K_{\mu}(t)$ satisfy $\sum_{\mu} K_{\mu}^{\dagger} K_{\mu} = I$ for all t [2, 47]. For the atom-in-cavity model, they are explicitly given by

$$K_1 = \begin{bmatrix} \gamma & 0 \\ 0 & 1 \end{bmatrix} \otimes \begin{bmatrix} \gamma & 0 \\ 0 & 1 \end{bmatrix}, \tag{39}$$

$$K_2 = \begin{bmatrix} \gamma & 0 \\ 0 & 1 \end{bmatrix} \otimes \begin{bmatrix} 0 & 0 \\ \omega & 0 \end{bmatrix}, \tag{40}$$

$$K_3 = \begin{bmatrix} 0 & 0 \\ \omega & 0 \end{bmatrix} \otimes \begin{bmatrix} \gamma & 0 \\ 0 & 1 \end{bmatrix}, \tag{41}$$

$$K_4 = \begin{bmatrix} 0 & 0 \\ \omega & 0 \end{bmatrix} \otimes \begin{bmatrix} 0 & 0 \\ \omega & 0 \end{bmatrix} \tag{42}$$

where $\gamma = \exp(-\Gamma t/2)$ and $\omega = \sqrt{1 - \exp(-\Gamma t)}$.

It is possible to choose intial states such that the density matrices have the following form for all t

$$\rho(t) = \frac{1}{3} \begin{bmatrix} a(t) & 0 & 0 & 0\\ 0 & b(t) & z(t) & 0\\ 0 & z(t) & c(t) & 0\\ 0 & 0 & 0 & d(t) \end{bmatrix}$$
(43)

with

$$a(t) = \kappa^2 a_0, \tag{44}$$

$$b(t) = c(t) = \kappa + \kappa (1 - \kappa) a_0, \tag{45}$$

$$d(t) = 1 - a_0 + 2(1 - \kappa) + (1 - \kappa)^2 a_0, \tag{46}$$

$$z(t) = \kappa. \tag{47}$$

where $\kappa = \exp(-\Gamma t)$.

The two-qubit entanglement is

$$C^{AB}(t) = \frac{2}{3} \max\{0, \kappa f(t)\},$$
 (48)

where $f(t) = 1 - \sqrt{a_0[1 - a_0 + 2(1 - \kappa) + (1 - \kappa)^2 a_0]}$.

In the coherence vector representation, the non-zero components are

$$n_{IZ}(t) = n_{ZI}(t) = -1 + \frac{2}{3}(1 + a_0)\kappa$$
 (49)

$$n_{XX}(t) = n_{YY}(t) = \frac{2}{3}\kappa \tag{50}$$

$$n_{ZZ}(t) = 1 - \frac{4}{3}(1 + a_0)\kappa + \frac{4}{3}a_0\kappa^2.$$
 (51)

and the limiting state is

$$\vec{n}_{\infty} = (-1, 0, 1),$$
 (52)

where the coordinates are (n_{IZ}, n_{XX}, n_{ZZ}) .

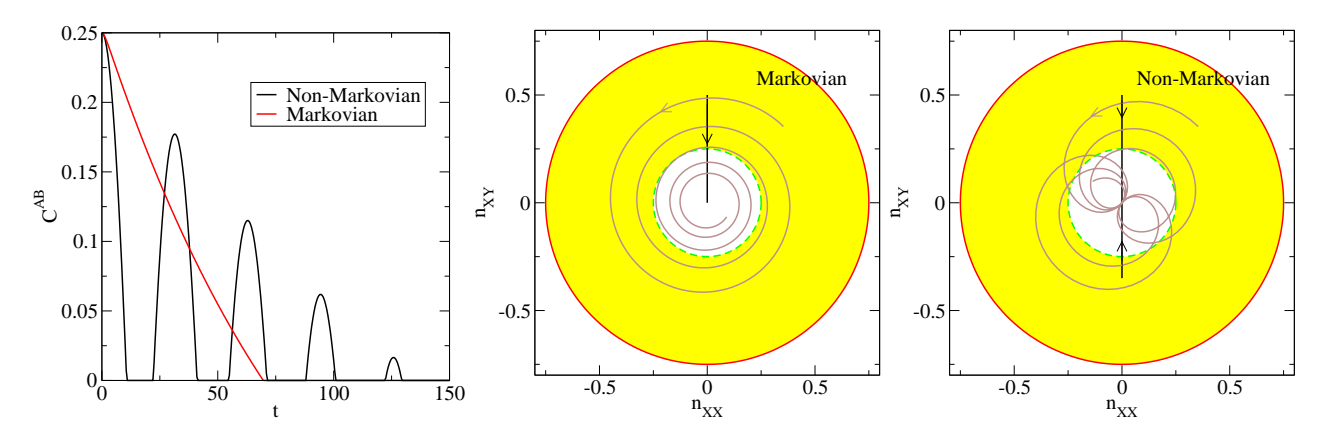


FIG. 8. (Color online) Entanglement evolution in ZJ_5 with pure dephasing noise. Only one qubit is subject to RTN and the other sees a static field B_0 . State trajectories with intial state $w_r^{\Psi^+}$ is colored brown while those with intial state $w_r^{\Phi^+}$ are colored black. $\gamma = 0.5, g = 0.1, r = 0.5, B_0 = 0.1$.

The positivity condition for the density matrix is given by

$$\begin{aligned} a_2 &\geq 0 \Rightarrow 2n_{IZ}^2 + 2n_{XX}^2 + n_{ZZ}^2 \leq 3 \\ a_3 &\geq 0 \Rightarrow 2n_{IZ}^2 + 2n_{XX}^2 + n_{ZZ}^2 \leq 1 + 2n_{ZZ} \left(n_{IZ}^2 - n_{XX}^2 \right) \\ a_4 &\geq 0 \Rightarrow AB \geq 0 \end{aligned}$$

where $A = (1+n_{ZZ})^2 - 4n_{IZ}^2$ and $B = (1-n_{ZZ})^2 - 4n_{XX}^2$. The square roots of the eigenvalues of $\rho\tilde{\rho}$ are

$$\lambda_a = \lambda_b = \frac{1}{4}\sqrt{A} \tag{53}$$

$$\lambda_c = \frac{1}{4} |1 - n_{ZZ} + 2n_{XX}| \tag{54}$$

$$\lambda_d = \frac{1}{4} |1 - n_{ZZ} - 2n_{XX}| \tag{55}$$

To compute concurrence, one needs to decide the ordering of these λ 's. A simple fact is that λ_a being the largest leads to $C^{AB} = 0$.

The dynamical subspace YE_5 is a tetrahedron with vertices at (0, -1, -1), (0, 1, -1), (-1, 0, 1), and (1, 0, 1), as seen in Fig. 9. $YE_5 \cap S$ is a hexahedron that shares some external areas with YE_5 . Two dimensional section of YE_5 with $n_{IZ} = 0$ is exactly the same as Fig. 7. On the other hand, if the section is done with $n_{XX} = 0$, we get a upside down triangle made of separable states, as shown in Fig. 10.

Yu and Eberly showed that a sudden transition of the entanglement evolution from category \mathcal{A} to category \mathcal{E} is possible as one tunes the physical parameter a_0 . This phenomenon can be easily understood in our formalism, as seen in Fig. 11. The curvature of the state trajectories vary as the initial state changes. Thus there is a continuous range of initial states parametrized by a_0 whose trajectories enter S within finite amount of time and also a continuous range of initial states whose trajectories never enter S. Note Fig. 11 is a skematic drawing since the true state trajectories are truely three dimensional.

Note the limiting state \vec{n}_{∞} of this model is on the boundary of the entangled and separable regions. It is

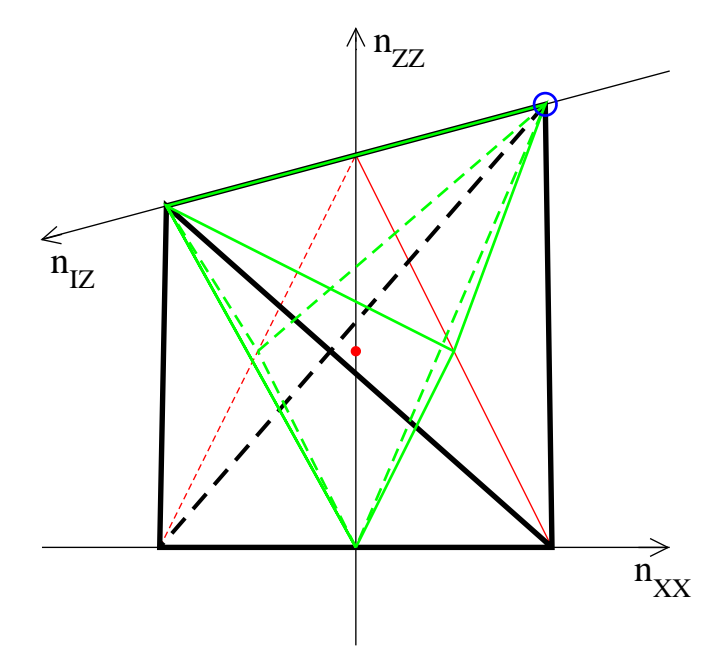


FIG. 9. (Color online) The dynamical subspace YE_5 is a tetrahedron outlined by black lines. The set of separable states $YE_5 \cap S$ form a hexahedron outlined by green lines. The origin (fully mixed state $\vec{n} = \mathbf{0}$) is denoted by a red filled dot. The limiting state \vec{n}_{∞} in Ref. [7] is denoted by a blue circle.

the reason that entanglement evolutions in both category \mathcal{A} and category \mathcal{E} are possible.

VIII. CONCLUSIONS

In conclusion, we classified entanglement evolutions into four categories using a geometrical picture constructed by coherence (generalized Bloch) vector representation. Two factors of any physical model, the dynamical subspace D and the limiting state of the dynam-

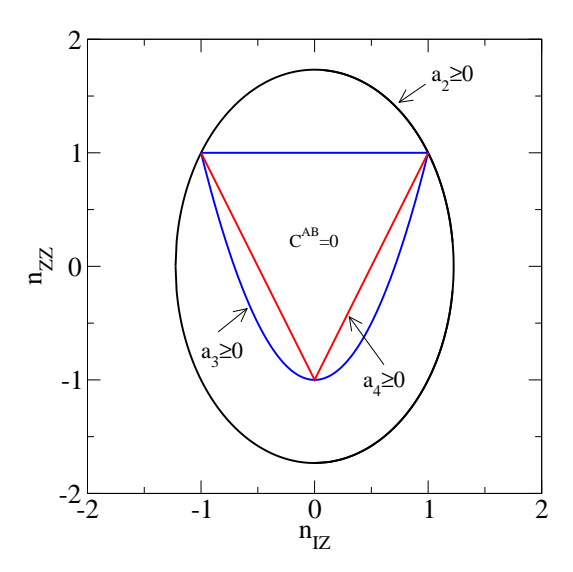


FIG. 10. (Color online) Cross section of the dynamical subspace YE_5 with $n_{XX}=0$. $a_2\geq 0$ is the eclipse. $a_3\geq 0$ gives the parabola and the top of the isoceles triangle. $a_4\geq 0$ sets the two sides of the triangle. The whole section is filled with separable states.

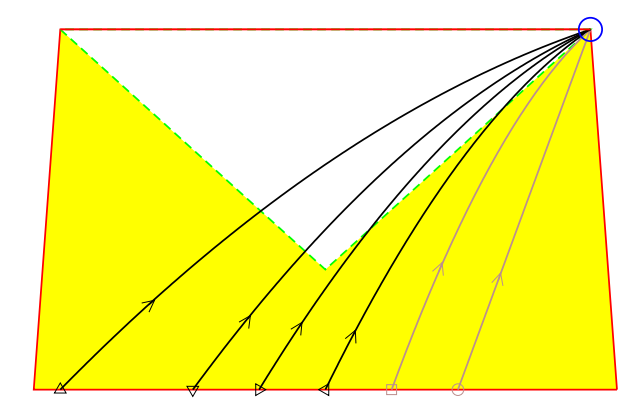


FIG. 11. (Color online) Skematic drawing of the different types of entanglement evolutions in the dynamical subspace YE_5 . The limiting state \vec{n}_{∞} is denoted by a blue circle on the top right corner. Entanglement evolutions in category \mathcal{A} are brown-colored while those in category \mathcal{E} are black-colored.

ics \vec{n}_{∞} are most important in determining the categories which the model supports. Dynamical subspaces with trivial entanglement topology, that is, $D \cap S$ is of zero volume in D, can only support entanglement evolutions in categories \mathcal{A} and \mathcal{B} . Whereas D with non-trivial entanglement topology can have entanglement evolutions in all four categories. For a dynamical subspace with non-trivial entanglement topology to have entanglement evolutions in categories \mathcal{A} and \mathcal{B} , the limiting state \vec{n}_{∞} has to be on the boundary of S. The memory effect of the noise also plays a role in determining the entanglement evolution. Generally speaking, Markovian noise tends to cause evolutions in categories \mathcal{A} and \mathcal{E} while non-Markovian noise tends to induce evolutions in categories \mathcal{B} and \mathcal{O} .

ACKNOWLEDGMENTS

We thank Amrit De, Alex Lang and Andre L. Saraiva for helpful discussions. This work was supported by Grant NSF-ECS-0524253 and NSF-DMR-0805045, by the DARPA QuEST program, and by ARO and LPS Grant W911NF-08-1-0482.

R. Horodecki, P. Horodecki, M. Horodecki, and K. Horodecki, Rev. Mod. Phys., 81, 865 (2009).

^[2] M. A. Nielsen and I. L. Chuang, Quantum Computation and Quantum Information, 1st ed. (Cambridge University Press, 2000).

 ^[3] S. Hill and W. K. Wootters, Phys. Rev. Lett., 78, 5022
 (1997); W. K. Wootters, *ibid.*, 80, 2245 (1998); Quantum Information and Computation, 1, 27 (2001).

^[4] T. Yu and J. H. Eberly, Science, 323, 598 (2009).

^[5] M. P. Almeida, F. de Melo, M. Hor-Meyll, A. Salles, S. P. Walborn, P. H. S. Ribeiro, and L. Davidovich, Science,

³¹⁶, 579 (2007); J. Laurat, K. S. Choi, H. Deng, C. W. Chou, and H. J. Kimble, Phys. Rev. Lett., **99**, 180504 (2007); J.-S. Xu, C.-F. Li, M. Gong, X.-B. Zou, C.-H. Shi, G. Chen, and G.-C. Guo, **104**, 100502 (2010).

^[6] K. Zyczkowski, P. Horodecki, M. Horodecki, and R. Horodecki, Phys. Rev. A, 65, 012101 (2001).

^[7] T. Yu and J. H. Eberly, Phys. Rev. Lett., 93, 140404 (2004).

^[8] T. Yu and J. H. Eberly, Phys. Rev. Lett., 97, 140403 (2006); T. Yu and J. Eberly, Optics Communications, 264, 393 (2006); 283, 676 (2010).

- [9] J.-H. Huang and S.-Y. Zhu, Phys. Rev. A, **76**, 062322 (2007).
- [10] X. Cao and H. Zheng, Phys. Rev. A, 77, 022320 (2008).
- [11] A. Al-Qasimi and D. F. V. James, Phys. Rev. A, 77, 012117 (2008).
- [12] M. Hernandez and M. Orszag, Phys. Rev. A, 78, 042114 (2008).
- [13] K. Roszak, P. Horodecki, and R. Horodecki, Phys. Rev. A, 81, 042308 (2010).
- [14] M. Al-Amri, G.-x. Li, R. Tan, and M. S. Zubairy, Phys. Rev. A, 80, 022314 (2009).
- [15] M. Ikram, F.-l. Li, and M. S. Zubairy, Phys. Rev. A, 75, 062336 (2007).
- [16] A. Vaglica and G. Vetri, Phys. Rev. A, 75, 062120 (2007).
- [17] J. León and C. Sabín, Phys. Rev. A, 79, 012301 (2009).
- [18] B. Bellomo, R. Lo Franco, and G. Compagno, Phys. Rev. Lett., 99, 160502 (2007); Phys. Rev. A, 77, 032342 (2008).
- [19] D. Zhou, A. Lang, and R. Joynt, Quantum Information Processing (2010), doi:10.1007/s11128-010-0165-2.
- [20] Z. Ficek and R. Tanaś, Phys. Rev. A, 74, 024304 (2006); L. Mazzola, S. Maniscalco, J. Piilo, K.-A. Suominen, and B. M. Garraway, 79, 042302 (2009); C. E. López, G. Romero, F. Lastra, E. Solano, and J. C. Retamal, Phys. Rev. Lett., 101, 080503 (2008).
- [21] M. Yönaç, Т. Yu, and J. Η. Eberly. Journal of Physics B: Atomic, Molecular and Optical Physics 4298 State (2006) vectronic Noise and Fluctuations in Solids M. Yönaç and J. H. Eberly, Opt. Lett., 33, 270 (2008).
- [22] K. Ann and G. Jaeger, Phys. Rev. A, 76, 044101 (2007).
- [23] Y. S. Weinstein, Phys. Rev. A, 79, 012318 (2009); 79, 052325 (2009); **80**, 022310 (2009).
- [24] L. Aolita, R. Chaves, D. Cavalcanti, A. Acín, L. Davidovich, Phys. Rev. Lett., 100, 080501 (2008).
- [25] C.-Y. Lai, J.-T. Hung, C.-Y. Mou, and P. Chen, Phys. Rev. B. 77, 205419 (2008).
- [26] J. P. Paz and A. J. Roncaglia, Phys. Rev. Lett., 100. 220401 (2008); Phys. Rev. A, **79**, 032102 (2009).
- [27] S.-Y. Lin, C.-H. Chou, and B. L. Hu, Phys. Rev. D, 78, 125025 (2008).
- [28] R. Vasile, S. Olivares, M. G. A. Paris, and S. Maniscalco, Phys. Rev. A, 80, 062324 (2009).

- [29] T. Yu and J. H. Eberly, JOURNAL OF MODERN OP-TICS, 54, 2289 (2007).
- [30] M. O. Terra Cunha, New Journal of Physics, 9, 237 (2007).
- [31] D. Zhou (2010),and R. Joynt, arXiv:1006.5474 [quant-ph].
- [32] K. Zyczkowski, P. Horodecki, A. Sanpera, and M. Lewenstein, Phys. Rev. A, 58, 883 (1998).
- G. Kimura, Physics Letters A, 314, 339 (2003); M. S. Byrd and N. Khaneja, Phys. Rev. A, 68, 062322 (2003).
- [34] G. Mahler and R. Wawer, Quantum Networks: Dynamics of Open Nanostructures, 2nd ed. (Springer, 1998); R. Alicki and K. Lendi, Quantum dynamical semigroups and applications (Springer-Verlag, 1987).
- [35] R. Joynt, Zhou. Q.-H. D. Wang, arXiv:0906.2843 [quant-ph].
- C. Drumond and M. Ο. Т. Journal of Physics A: Mathematical and Theoretical, 42, 285308 (20
- [37] A. De, A. Lang, D. Zhou, and R. Joynt, arXiv:1006.5943 [cond-mat].
- [38] H. Braga, S. Souza, and S. S. Mizrahi, Phys. Rev. A, **81**, 042310 (2010).
- [39] R. Horodecki and M. Horodecki, Phys. Rev. A, 54, 1838 (1996).
- [40]R. F. Werner, Phys. Rev. A, 40, 4277 (1989).
- [41] L. Jakbczyk and M. Siennicki, Physics Letters A, 286, 383 (2001), ISSN 0375-9601.
- (Cambridge University Press, 2008).
- [43] R. C. Bialczak, R. McDermott, M. Ansmann, M. Hofheinz, N. Katz, E. Lucero, M. Neeley, A. D. O'Connell, H. Wang, A. N. Cleland, and J. M. Martinis, Phys. Rev. Lett., 99, 187006 (2007).
- [44] J. Bergli, Y. M. Galperin, and B. L. Altshuler. New Journal of Physics, 11, 025002 (2009).
- [45] B. Cheng, Q.-H. Wang, and R. Joynt, Phys. Rev. A, 78, 022313 (2008); D. Zhou and R. Joynt, 81, 010103 (2010).
- [46] L. Gurvits and H. Barnum, Phys. Rev. A, 68, 042312 (2003); **72**, 032322 (2005).
- [47] K. Kraus, A. Bohm, J. D. Dollard, and W. H. Wootters, States, effects, and operations: fundamental notions of quantum theory (Springer-Verlag, 1983).